Materials Science and Engineering A 545 (2012) 97–102

Contents lists available at SciVerse ScienceDirect

Materials Science and Engineering A

journal homepage: www.elsevier.com/locate/msea

Microstructural features and mechanical properties of Al 5083/SiC_p metal matrix nanocomposites produced by high energy ball milling and spark plasma sintering

Sivaiah Bathula*, R.C. Anandani, Ajay Dhar, A.K. Srivastava

CSIR-National Physical Laboratory, Dr. K.S. Krishanan Marg, New Delhi 110012, India

ARTICLE INFO

Article history:
Received 8 January 2012
Received in revised form 27 February 2012
Accepted 29 February 2012
Available online 13 March 2012

Keywords:
Powder metallurgy
Electron microscopy
Al 5083/10 wt.% SiC_p nanocomposite
Spark plasma sintering
Interfaces

ABSTRACT

Al 5083 alloy powder with 10 wt.% (~8.43 vol.%) of silicon carbide (SiC_p) nanoparticulates having size of ~20 nm were milled using a high-energy planetary ball mill to produce Al 5083/10 wt.% SiC_p (Al 5083/SiC_p) nanocomposite. Subsequently, the milled powders were consolidated and sintered by employing spark plasma sintering (SPS) technique in order to attain the near theoretical densification while retaining the nanostructure of Al 5083 matrix embedded with uniformly distributed SiC_p. High resolution transmission microscopy (HR-TEM) analysis revealed the grain morphology and grain size of the Al 5083 matrix along with the interfacial microstructure between Al 5083 matrix and SiC_p particulates. The crystallite size of ball milled Al 5083 matrix was observed to be ~25 nm and was coarsened up to 30 nm after rapid consolidation and sintering using SPS. Compressive strength and elastic modulus of Al 5083/SiC_p metal matrix nanocomposites was significantly increased to that of the un-reinforced Al 5083 alloy. Nanoindentation measurements on these nanocomposites demonstrated the hardness of ~280 HV with an elastic modulus of 126 GPa.

1. Introduction

Al alloy/SiC_p based nanocomposites are finding numerous applications in the design and construction of automobile and aerospace structures, which possess high strength and elastic modulus [1]. Al based composites are important for manufacturing brake drums, cylinder liners, cylinder blocks, drive shafts, rotor vanes, rotor plates in automobile and as well an in aerospace industries [2,3]. Al 5083 alloy has been chosen for this study because of its high strength and non-heat-treatable in commercial use. It has good weldability, formability, excellent tensile strength and corrosion resistance. These properties are desirable for structural applications requiring high strength and moderate ductility. In general, nanocomposites are the materials that incorporate nano-sized ceramic particles into the matrix of standard alloy, which results in drastic improvement in properties such as mechanical strength, toughness in Al based composites, etc. [4]. There are quite a few methods available to synthesize metal matrix composites in bulk quantity at inexpensive production cost, e.g., squeeze casting [5], liquid metal infiltration [6] and ball milling. In the case of squeeze casting and infiltration methods, the addition of nanoparticles to the melt leads to inhomogenity of second phase distribution in the matrix, due to their poor wettability and the formation of undesired intermetallic phases and undesired residual porosity. Ball milling [7] is a technique for the production of nanocomposite powders. The action of re-welding and fracturing of ceramic and metallic powders in a highly activated milling media leads to achieve ultrafine grained or nanostructures in the matrix.

Subsequently the powders are consolidated and sintered by various conventional sintering techniques. However, conventional sintering of nanocomposites with longer duration of sintering cycles leads to excess grain growth in the material, due to the excess free energy associated with the large amount of grain boundary area of the nanostructured matrix, which thermodynamically favours grain growth. It is well recognized that the pressure, temperature and sintering time are the critical parameters for consolidation and sintering of nanocomposite powders. There are few approaches available in the literature for consolidation and sintering of nanocomposites such as, hot pressing, hot isostatic pressing (HIPing), resistance sintering process and spark plasma sintering (SPS), etc. HIPing technique was used [8] for the densification of nanostructured materials. The densification was associated to the nucleation and growth of neck formation at contact points that fill up the pores accomplished by plastic deformation during application of stress associated with power-law creep and mass diffusion to the remaining free surfaces. The grain growth of the materials would lead to near theoretical densification, however, it adversely affects the mechanical properties. The same sintering technique was used for consolidation of cryomilled Al 5083/SiC_p nanocomposite powders [9] had a grain size of the order of 30 nm and it was

* Corresponding author. Tel.: +91 11 45608443; fax: +91 11 45609310.
E-mail addresses: bsivaiah@gmail.com, sivaiahb@mail.nplindia.org (S. Bathula).

0921-5093/$ – see front matter © 2012 Elsevier B.V. All rights reserved.
doi:10.1016/j.msea.2012.02.095

increased to 100–200 nm. The microstructure had shown bimodal distribution of grain sizes with the inter-particle regions formed via elemental diffusion due to longer duration of HIP sintering cycle. The higher sintering temperatures in HIPing improved the wettability of SiC_p with matrix of Al alloys, however, it resulted in the formation of Al_4C_3 and free silicon at interface reducing the crack toughness properties of bulk material. Similar rapid sintering technique such as, resistance sintering [10] was used to consolidate Al/SiC_p nanocomposites at higher heating rates and shorter sintering (~1 s) cycles to produce high strength nanocomposites. This technique resulted in narrow pores and voids in the microstructure that limits the densification. These constraints can minimized to lowest possible extent with the use of rapid sintering technique such as SPS and this technique was the most successful for consolidation and sintering of nanocomposite powders for obtaining near theoretical densification with enhanced mechanical properties. The rapid heating rates and shorter sintering cycles with simultaneous application of load avoids grain growth in nanocomposites on the composite powders are favoured to have prohibition in terms of grain growth.

In the present investigation we adapted a ball milling technique followed by SPS to synthesize the Al 5083/10 wt.% SiC_p nanocomposite in bulk with improved mechanical properties. The absence of pores and voids in the microstructure with near theoretical density has been demonstrated and discussed. Mechanical characteristics by evaluating the data of nanoindentation delineated the hardness and strength profiles of these composites in the matrix and matrix/SiC_p interface as well.

2. Experimental procedure

Al 5083 alloy (Al–4.5Mg, 0.9Mn, 0.4Mn, 0.4Si, 0.2Cu, 0.15Ti, 0.25Zn) powder having a size ~15 μm (density: 2.66 g/cm^3) was ball milled along with 10 wt.% of SiC_p nanoparticulates of size ~20 nm (density: 3.21 g/cm^3) in a *Fritsch* make *Pulverisette-4* ball mill for 15 h. The vial of the ball-mill and the milling media were made up of stainless steel. The ball-to-powder weight ratio was maintained at 20:1 and milled in argon atmosphere with a milling speed of 400 rpm for 5 min on- and off-cycles, respectively. In order to prevent the re-welding and promote the fracturing of powder particles, 2 wt.% of stearic acid was added as a process control agent. Prior to consolidation and sintering, ball milled nanocomposite powder was kept in *Mbraun make* glove box to minimize oxidation and other atmospheric contamination.

Crystallite size measurements were carried out using an X-ray diffractometer (model: *D8 Advanced*, make: *Bruker*). In order to calculate the final crystallite size of milled powders, full width half maxima (FWHM) values were subtracted for instrumental broadening and $K\alpha_2$ corrections. Average crystallite size was calculated using *Scherrer* and *Williamson–Hall* methods by considering four high intensity peaks obtained for Al 5083 matrix, i.e., (1 1 1), (2 0 0), (2 2 0) and (3 1 1). Nanocomposite powders of Al5083/10 wt.% SiC_p were subsequently consolidated and sintered under vacuum (~4 Pa) using SPS (model: *SPS 725*, make: *Dr. Sinter, Japan*) at a pressure of 50 MPa, at 500 °C for 3 min using graphite die and punches. The heating rate was maintained at 300 °C per min. The surface morphology of ball milled powders and sintered pellets were studied by scanning electron microscope (SEM model: *EVO MA10*, make: *Zeiss*). Micro hardness measurements were done using Vickers microhardness tester (model: *FM-e7*) with a load of 100 g for 10 s of indentation time. The density of composites was measured by conventional Archimedes principle. High resolution transmission microscopy (HR-TEM, Model: *Tecnai G2 F 30 STWIN, FEG source, electron accelerating voltage 300 kV*) was carried out on milled powders and SPS samples to study the

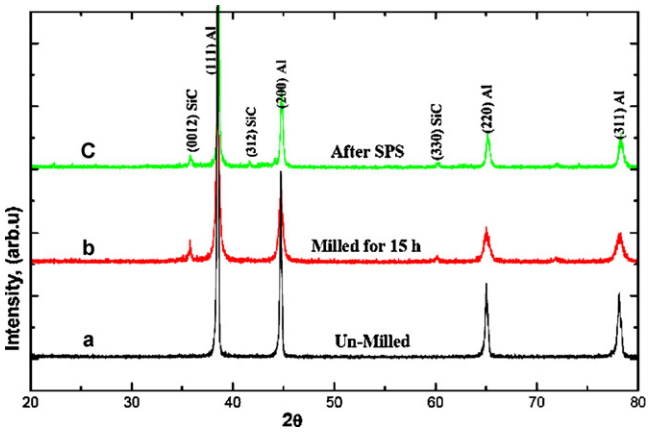

Fig. 1. (a) XRD peak profile of (a) un-milled Al 5083 alloy, (b) Al 5083/SiC_p high energy ball milled for 15 h and (c) Al 5083/SiC_p after SPS process.

dispersion of different nano-constituents in the matrix and the interface of Al 5083/SiC_p nanocomposites. Elastic modulus and hardness measurements were performed using nanoindentation technique (*M/s Fischer-Cripps Laboratories Pvt. Limited, Australia*) at a load of 50 mN. The mechanical properties were derived from the measured load–penetration depth curves under loading/unloading through standard data analysis software. Compression test has been performed at room temperature as per ASTM standard (ASTM E9-09) with a length/diameter ratio of 2.0 using *INSTRON 4204* testing facility under uni-axial loading with a strain rate of 5×10^{-5} s^{-1}.

3. Results and discussion

X-ray diffraction analyses (XRD) were carried out for un-milled, milled for 15 h and SPS derived Al 5083/SiC_p nanocomposites. *Scherrer* and *Williamson–Hall* methods [11] were used to calculate crystallite size and lattice strain of the Al 5083 matrix. The characteristic XRD peak profile shown in Fig. 1 indicates a sharp decrease in peak intensity with an increased peak broadening for the powders ball milled for 15 h. It is known that the impact and shear forces of milling media induces crystalline defects such as dislocations and stacking faults [12]. This further leads to increase in the stored energy of the system up to a critical value. Beyond this, reduction of energy takes place by forming sub-grains and high angle grain boundaries over the entire volume of milling powder leading to nanostructure. The final grain size of Al 5083 matrix composite powders depends primarily on SiC_p content and the milling time [13]. The average crystallite size and lattice strain were measured to be ~25 nm and 0.43 respectively, after 15 h of high energy ball milling. The SEM micrographs of both as-received and milled powders for 15 h have been shown in Fig. 2(a) and (b). The powders at the starting stage of milling were spherical in shape with an average size of 15 μm and the ball milled powders have shown facetted morphology with the particle size between ~40 and 50 μm (Fig. 2(b)). The increase in particle size could be explained on the basis of welding of particles at the first instant followed by fracture at the second [14]. During milling, the hard particles of SiC_p nanoparticles were distributed homogeneously as shown in Fig. 3(a) and are embedded into the deformed Al 5083 soft matrix forming agglomerated particles of Al 5083/SiC_p composite powders (Fig. 3(b)). It is further to note that the energy dispersive X-ray analysis (EDX) analysis did not reveal any evidence of the formation of reactive products such as Al_4C_3 and free silicon after 15 h of milling. This is further to mention that EDS analysis showed the dispersion of SiC nanoparticulates in Al 5083 alloy matrix (Fig. 3(c)). High resolution TEM bright-field images (Fig. 4) of ball milled Al 5083/SiC_p

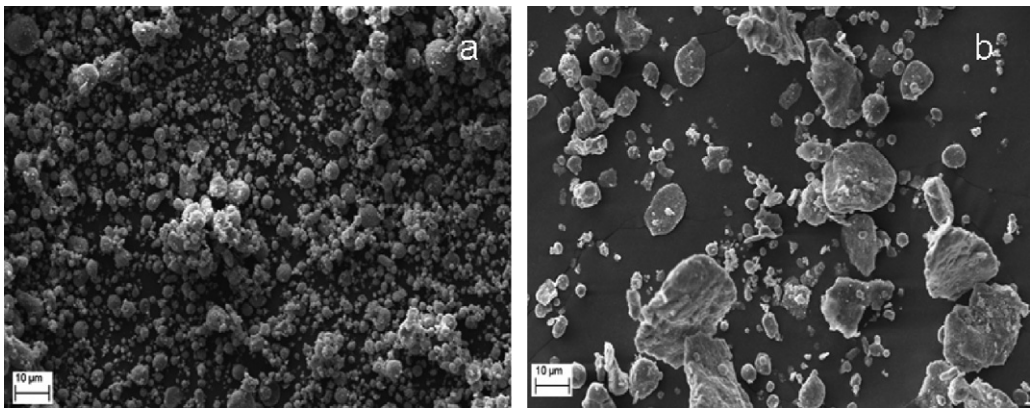

Fig. 2. SEM images of Al 5083/SiC_p powders after (a) un-milled Al 5083 alloy and (b) Al 5083/SiC after 15 h of high energy ball milling.

nanocomposite powders depicted the average grain size of ~28 nm with a homogeneous dispersion of SiC_p.

A detailed microscopy of SPS nanocomposites elucidated some important features at nano and lattice scale. It is known that SPS technique works mainly based on the electric spark discharge, where a high energy pulsated current momentarily generate spark plasma between the particles resulting in highly localized temperatures. It is recognized that the heat generated at the point contacts of the particles vaporize contaminants and break the oxide layer on the surface of Al 5083 particles prior to neck formation [15]. In the present work, the high resolution SEM images of spark plasma sintered Al 5083/SiC_p nanocomposite shown in Fig. 5(a) and (b) indicates the nano-sized SiC_p distributed uniformly in the Al 5083 matrix. The rapid heating rates of SPS resulted in the

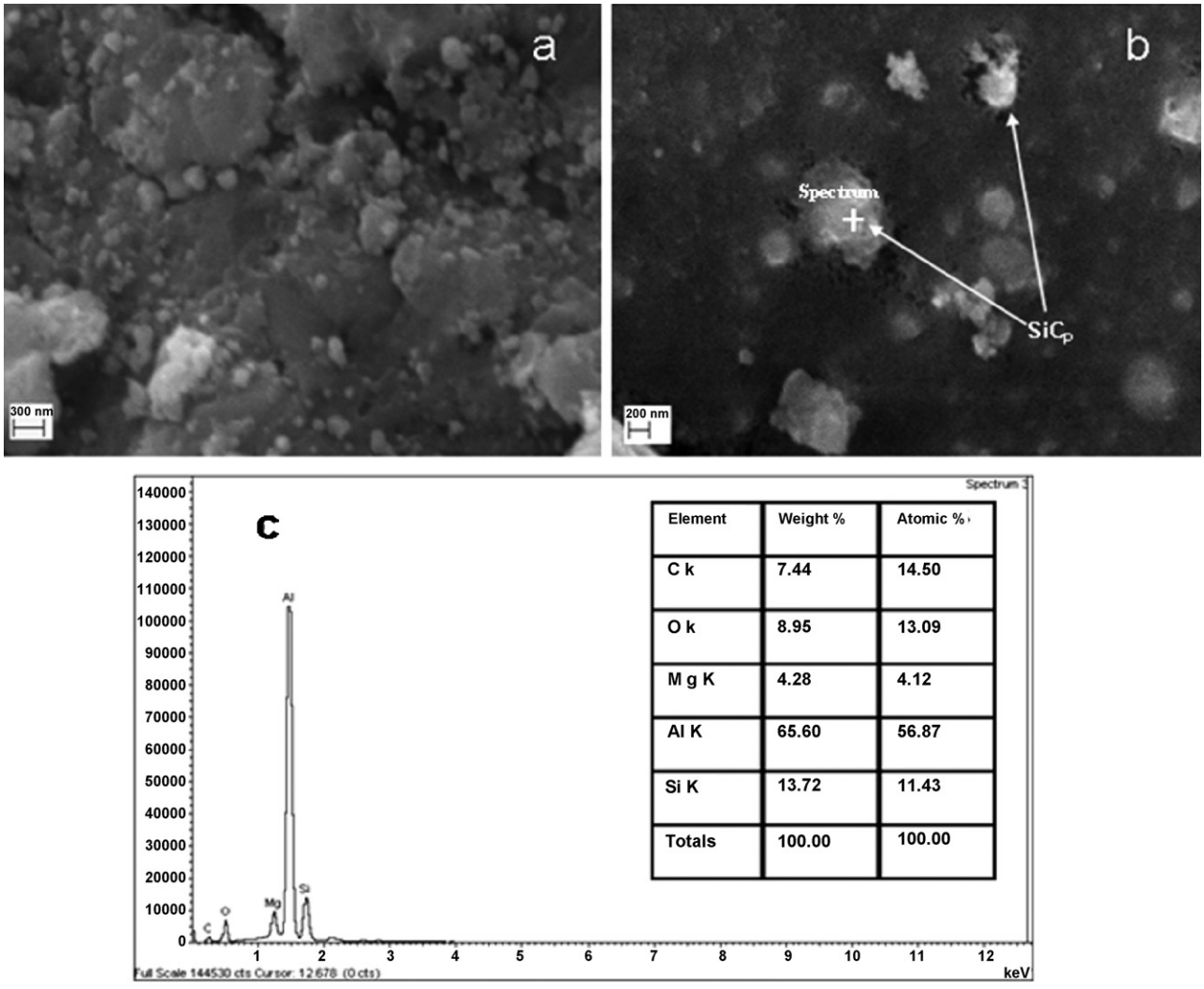

Element	Weight %	Atomic %
C k	7.44	14.50
O k	8.95	13.09
M g K	4.28	4.12
Al K	65.60	56.87
Si K	13.72	11.43
Totals	100.00	100.00

Fig. 3. (a, b) SEM images of Al 5083/SiC_p powders after 15 h of high energy ball milling, showing the dispersion of SiC_p and (c) EDS spectrum of SiC particle as indicated in (b).

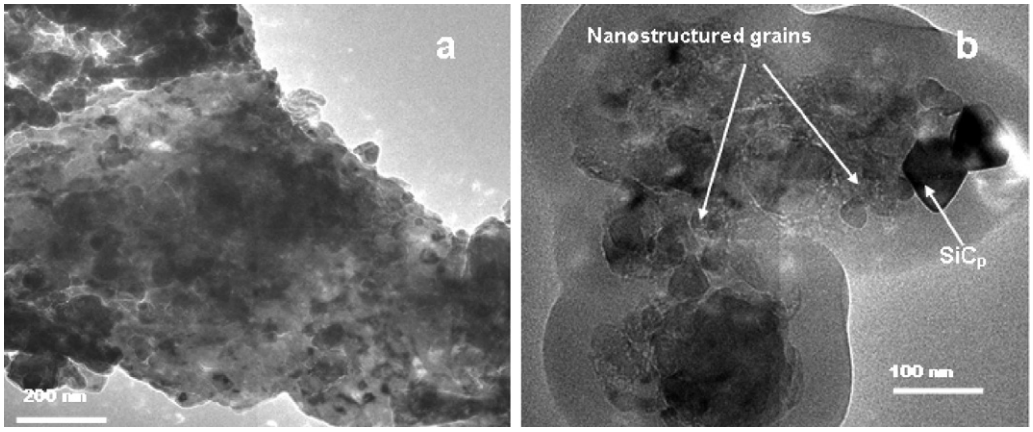

Fig. 4. (a, b) TEM bright-field images of Al 5083/SiC_p powders after 15 h of high energy ball milling, showing SiC_p dispersion.

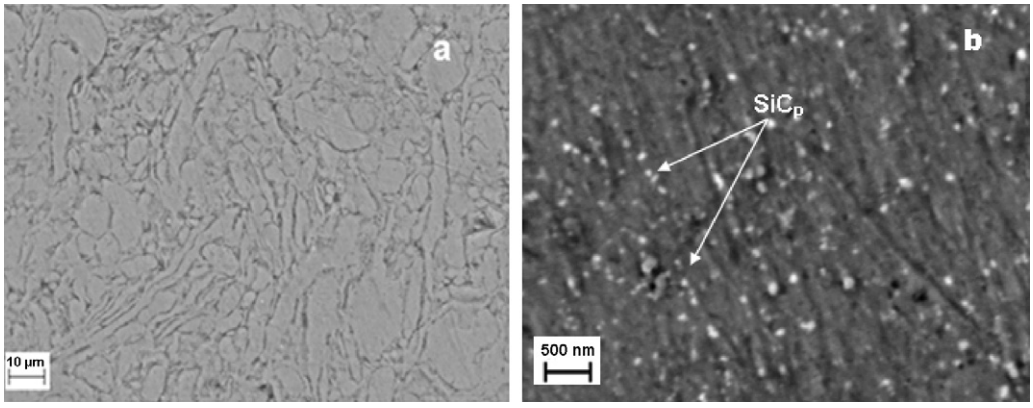

Fig. 5. (a, b) SEM images of spark plasma sintered Al 5083/SiC_p nanocomposite powders after SPS, showing minimum porosity.

formation of half-liquid and half-solid tendency in the Al 5083 particles with the simultaneous application of load. Due to the shorter sintering time cycle, the mass transport is limited and therefore the interior portion of the particles consisting of nanocrystalline grains remains unchanged. This leads to free flow ability of particles occupying the SiC_p nanoparticles regions containing the gaps/pores resulting in maximum densification. Apart from the reinforcement, neither voids nor cracks were detected and nanoparticles

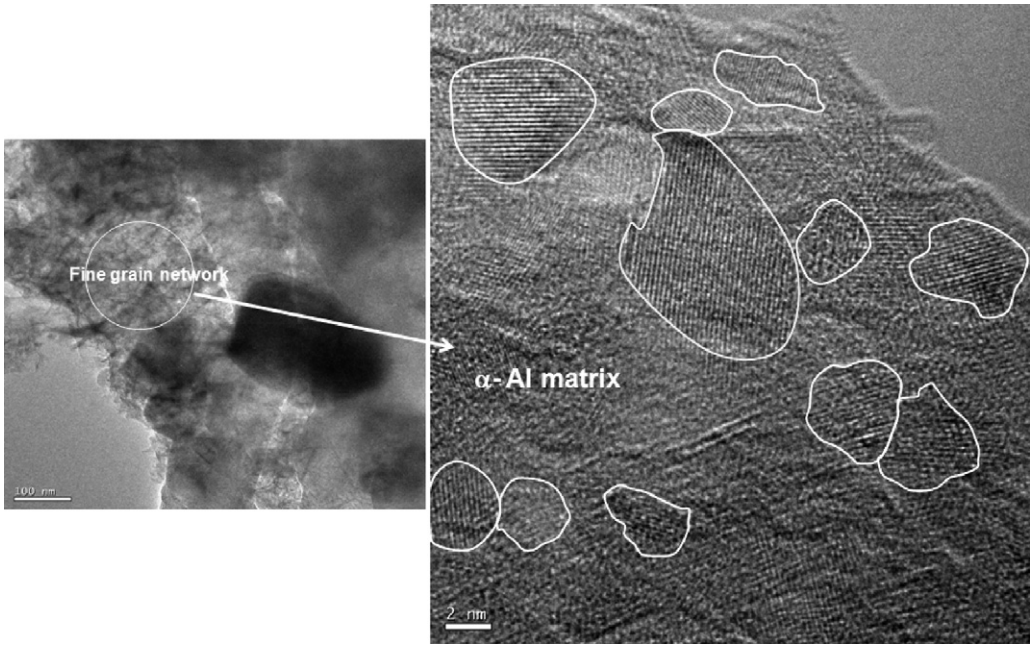

Fig. 6. HR-TEM image of spark plasma sintered Al 5083/SiC_p nanocomposite after SPS, showing large number of fine grains aligned in different directions.

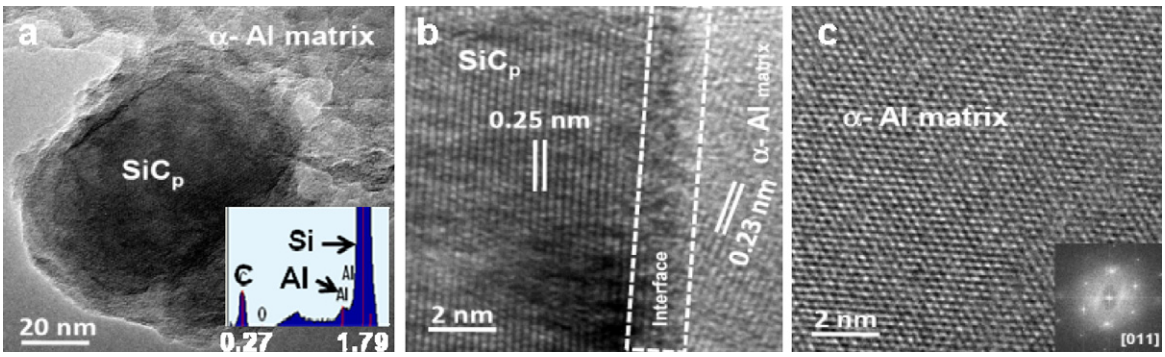

Fig. 7. HR-TEM images of spark plasma sintered Al 5083/SiCp nanocomposite after SPS, (a) large number of nanocrystalline grains over entire matrix of Al 5083 alloy along with a SiC_p, (b) interface between Al 5083 and SiC_p and (c) Al 5083 alloy matrix lattice imaging. Inset in (a) is EDAX spectrum showing the presence of C, Al and Si elements in the sample, X-axis: keV, Y-axis: intensity (arb. unit), inset in (c) shows corresponding FFT.

of SiC_p surrounded with the nanostructured Al 5083 grains have been clearly observed in Fig. 5(b). However, the high magnification micrographs recorded employing HR-TEM revealed a fine grained microstructure with the networked dislocations. A representative of such image is shown in Fig. 6. Further detailed analysis elucidated that a good interface was evolved around the SiC_p in the α-Al matrix (Fig. 7(a)). Moreover, there has been no visible porosity delineated at the interface around SiC_p even at nano-scale. The EDAX spectrum of the SiC nanoparticle dispersed in Al-matrix exhibits the presence of the peaks corresponding to C at 0.27 keV (energy level: $C_{K\alpha1,2}$ is 0.277 keV), Al at 1.49 keV (energy levels: $Al_{K\alpha}$ and $Al_{K\beta}$ are 1.487 and 1.553 keV) and Si at 1.79 keV (energy levels: $Si_{K\alpha1,2}$ and $Si_{K\beta}$ are 1.74 and 1.829 keV), as displayed in the inset of Fig. 7(a). The lattice scale imaging shown in Fig. 7(b) revealed that the planes of SiC_p (d-spacing: 0.25 nm) and Al 5083 (d-spacing: 0.23 nm) with an interface thickness of ~1.5–2 nm has been observed. One of the grains of Al 5083 matrix resolved at lattice scale had shown the arrangement of (1 1 1) planes through out the microstructure as shown in Fig. 7(c). The corresponding inset exhibits the fast Fourier transform (FFT) oriented along [0 1 1] zone axis, confirming the face centered cubic crystal (fcc) structure of α-Al. Apart from the retained nanostructure, there is no appearance of any intermetallics formation has been observed. Earlier results on Al 5083/5.97 wt.% SiC_p nanocomposite [16,17] prepared by cryomilling and consolidation by HIPing technique had shown dispersed SiC_p particles and free of SiC_p regions with bimodal grain size distribution in the microstructure. The reasons for SiC_p free regions are mainly attributed to elemental diffusion into the inter-particle pores during the HIPing process of longer sintering cycle. However, in the present work, SPS processed Al 5083/SiC_p nanocomposite exhibited homogeneous distribution of SiC_p in Al 5083 matrix due to the faster heating rates of SPS with shorter sintering cycles and the simultaneous application of load.

4. Mechanical properties and nanoindentation

Microhardness was recorded on Al 5083/SiC_p nanocomposite and nanostructured Al 5083 alloy has shown hardness values of ~250 and 148 HV, respectively. Significant enhancement in the compressive strength of ~824 MPa was observed for Al 5083/SiC_p nanocomposite due to dislocation pile-ups related to that of Orowan strengthening at grain boundaries. It is reasonable to admit that the shear band could not be formed in these composites, due to its difficulty in the dislocation movement through the dense SiC_p particulates dispersed in the nano-crystalline Al 5083 matrix [18]. As a result, the ductility of the nanostructured matrix reinforced with SiC_p regions was observed to be low. But, as per the inverse Hall–Petch effect, ductility in the nanomaterials is still possible with the reduction in grain sizes, which in turn results in a larger fraction of the atoms decorating the grain boundaries and suppressing the dislocation pile-ups. However, dislocation movement through multiple grains and sliding of grain boundaries becomes easier driven by high stress, even in the absence of thermally activated process [19]. Porosity level was very minimum for Al 5083/SiC_p nanocomposites after SPS, whereas for the sintered samples it was observed to be at the higher side as reported for HIPing technique [16]. Al 5083/SiC_p nanocomposites have achieved almost theoretical density, due to absence of void or crevice formation in our case.

Compressive strength test after SPS was conducted at room temperature under uni-axial compressive loading and stress–strain curves of the Al 5083 alloy and Al 5083/SiC_p were shown in Fig. 8. As sintered cylindrical samples with an L/D ratio of 2.0 were tested under uni-axial compression test between two flat and parallel platens. The relationship for the bulge correction factor was derived using an analytical procedure [20,21]. The bulge correction factor was used during the calculation of actual flow stress for un-reinforced and un-milled Al 5083 alloy along with nanostructured Al 5083 alloy and Al 5083/SiC_p nanocomposite. The bulge corrected flow stress values were shown in Fig. 8. The addition of the nanostructured reinforcement was found to be highly effective for improving the mechanical properties. A similar study [22] revealed that the average grain size was ~220 nm. Addition of SiC_p to the Al 5083 alloy had shown 26% increase in UTS, but a 92% decrease in elongation, in comparison with the tensile properties

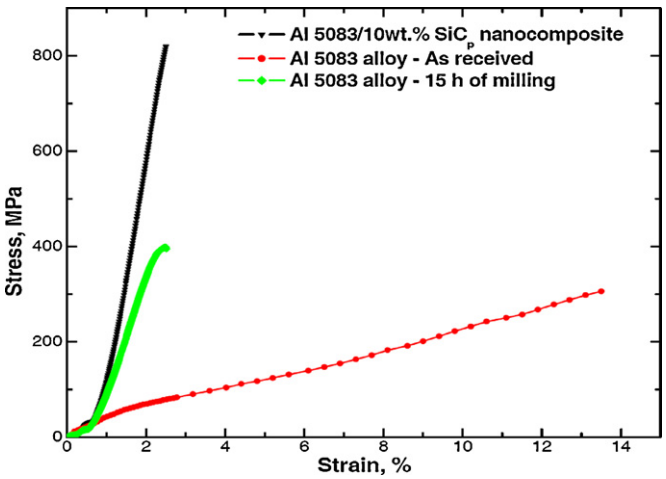

Fig. 8. Typical stress–strain curves from the compression test for un-milled Al5083 alloy, nanostructured Al 5083 alloy and Al 5083/SiC_p nanocomposite.

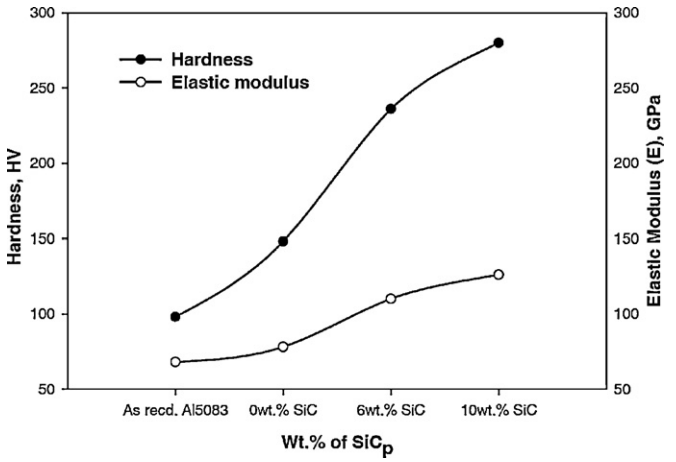

Fig. 9. Hardness and elastic modulus of the Al5083/SiC_p nanocomposite with the variation of SiC_p content.

reported for the nanocrystalline Al 5083 alloy [22]. In the present study, nanostructured Al 5083 alloy after 15 h of milling and with the addition of the 10 wt.% of SiC_p has been resulted in apparent increase of the compressive strength from 629 MPa to ~824 MPa, where as the compressive strength of un-reinforced and un-milled Al 5083 alloy was found to be 305 MPa. Percentage elongation was limited to 2.5% for Al 5083/SiC_p nanocomposite and it was observed 3.12% for nanostructured Al 5083 alloy as compared to that of 13.8% for Al 5083 alloy. The inferior ductility or the ductile instability was reported mainly due to the lack of strain hardening in nanocrystalline materials with the low activity of dislocations [23]. Ductility can also be improved by introducing coarse-grained regions in the nanocomposites, which increases the strain hardening effect and acts as crack arrester in turn improving the ductility of the material. However, introducing the coarse grained structure into the nanostructured materials significantly affects the tensile and compressive strength levels.

In order to study the elastic and plastic behavior of Al 5083/SiC_p nanocomposite at microscopic level nanoindentation test was performed [24]. This test was operated in the submicron depth range with nanometer resolution. The hardness and elastic modulus of Al 5083/SiC_p nanocomposite was evaluated from the load (50 mN)–penetration depth curves obtained in nanoindentation tests. Fig. 9 shows the enhancement in hardness and elastic modulus of the metal matrix nanocomposite with the variation of SiC_p content. Measured hardness and elastic modulus values for unmilled and un-reinforced Al 5083 alloy were found to be 98 HV and 68 GPa and by ball milling of Al 5083 alloy for 15 h, these values are enhanced to 148 HV and 78 GPa. With the addition of 10 wt.% SiC_p to Al 5083 alloy had shown significant improvement in hardness of ~280 HV and elastic modulus of 126 GPa. Hardness values of Al 5083/SiC_p nanocomposite obtained by Vickers microhardness tester was in good agreement with nano-indention hardness values. Similar behavior in other metal matrix nanocomposite [25] revealed that the addition of 20 vol.% Al_2O_3 to the Al 356 matrix increased the hardness and elastic modulus from 75 HV and 74 GPa to 216 HV and 86 GPa, respectively. Elastic modulus of the composites increased from 70 GPa for pure Al to 75 GPa and 85 GPa for the composites with 20 and 40 vol.% of $Al_{70}Ti_{20}Ni_{10}$ reinforcement, respectively [26]. In the present study, the enhancement of the mechanical properties with the addition of the nano-sized reinforcement has been observed with an improvement in the elastic modulus of the nanocomposites. The strength improvement was observed in the present case is similar to that of grain refinement and homogeneous dispersion of SiC_p resulted in effective inhibition of dislocation movement at matrix–particle interface [27]. In the present study Al 5083/SiC_p nanocomposite containing interface with a thickness of ~2 nm clearly indicates that the strengthening effect of particles in metal matrix nanocomposites is generally attributed from the load sharing mechanism by the applied stress directly from the matrix [28,29].

5. Conclusions

Al 5083/10 wt.% SiC_p metal matrix nanocomposites were successfully synthesized by employing ball milling followed by spark plasma sintering (SPS). These nanocomposites contained only α-Al and SiC phases with clear interface of thickness of ~1.5–2 nm and retained nano-grained network as evidenced by microscopy analysis. Further there was no evidence of formation of intermetallics has been observed due to the processing conditions we employed. The crystallite size of the ball milled Al 5083 matrix was observed to be ~25 nm and coarsened up to 30 nm after rapid consolidation and sintering using SPS. HRTEM investigations have shown homogeneous distribution of SiC_p and neither voids nor cracks are detected at the interface of Al 5083/SiC_p. Nanoindentation measurements on these metal nanocomposites demonstrated that the hardness of ~280 HV with an elastic modulus of 126 GPa and this was mainly due to the homogeneous dispersion of reinforcements and retained nano-grained microstructure of the matrix after SPS.

Acknowledgments

The authors are grateful to Director, CSIR-NPL for his support and facilities provided. The technical support rendered by Mr. K.N. Sood, Dr. N. Vijayan, Dr. Sushil Kumar, Dr. Sukhvir Singh and Dr. D. Haranath is gratefully acknowledged.

References

[1] E. Bonetti, L. Pasquini, E. Sampaolesi, Nanostruct. Mater. 9 (1997) 611.
[2] S. Sawla, S. Das, Wear 257 (2004) 555–561.
[3] Y. Sahin, Mater. Des. 28 (2007) 1348–1352.
[4] J.R. Davis, ASM Specialty Handbook: Aluminium and Aluminium Alloys, ASM International, 1993.
[5] Q. Zhang, G.Q. Chen, Z.Y. Xiu, M.H. Song, G.H. Wu, Mater. Lett. 57 (8) (2003) 1453–1458.
[6] H.S. Lee, S.H. Hong, Mater. Sci. Technol. 19 (2003) 1057.
[7] J.S. Benjamin, Metall. Trans. 1 (1970) 2943.
[8] H.V. Atkinson, S. Davies, Metall. Mater. Trans. A 31 (12) (2000) 2981–3000.
[9] P.M. Bronsveld, P. Bruinsma, J.Th. De Hosson, Mater. Sci. Eng. A 135 (1991) 77–81.
[10] S.J. Hong, et al., Mater. Sci. Eng. A 148 (1991) 189–195.
[11] B.D. Cullity, S.R. Stock, Elements of X-ray Diffraction, 3rd ed., Prentice-Hall Inc, 2001, pp. 167–171.
[12] R. Daly, M. Khitouni, A.W. Kolsi, N. Njah, Phys. Stat. Sol. (c) 3 (9) (2006) 3325–3331.
[13] E.M. Sherif, J. Alloys Compd. 279 (1998) 263–271.
[14] F.L Zhang, C.Y. Wang, M. Zhu, Scr. Mater. 49 (2003) 1123–1128.
[15] M.J. Yang, D.M. Zhang, X.F. Gu, L.M. Zhang, Mater. Chem. Phys. 99 (2006) 170–173.
[16] F. Tang, M. Hagiwara, J.M. Schoenung, Scr. Mater. 53 (2005) 619.
[17] B.Q. Han, Z. Lee, D. Witkin, S. Nutt, E.J. Lavernia, Metall. Mater. Trans. A 36A (2005) 1–9.
[18] H. van Swygenhoven, J.R. Weertman, Mater. Today 9 (24) (2006).
[19] J. Schiøtz, F.D. Di Tolla, K.W. Jacobsen, Nature 391 (5) (1998).
[20] O. Ettouney, D.E. Hardt, ASME J. Eng. Ind. 105 (1983) 161–167.
[21] E.M. Mielnik, Metalworking Science and Engineering, McGraw-Hill, 1991.
[22] F. Tang, et al., Mater. Sci. Eng. A 407 (2005) 306–314.
[23] D.G. Morris, Mechanical behavior of nanostructured materials, Trans Tech Publication Ltd., Uetikon-Zuerich, Switzerland, 1998, p. 19 (vol. 2).
[24] W.C. Oliver, G.M. Pharr, J. Mater. Res. 19 (12) (2004) 3–20.
[25] Y. Mazaheri, F. Karimzadeh, M.-H. Enayati, Mater. Sci. Appl. 1 (1) (2010) 217–222.
[26] S. Scudino, F. Ali, K.B. Surreddi, K.G. Prashanth, M. Sakaliyska, J. Eckert, J. Phys.: Conf. Ser. 240 (2010) 012154.
[27] D.J. Lloyd, Int. Mater. Rev. 39 (1) (1994) 1–24.
[28] M.R. Piggot, Load-Bearing Fiber Composites, Pergamon Press, Oxford, 1980.
[29] V.C. Nardone, Scr. Mater. 21 (1987) 1313.